PHYSICAL REVIEW C VOLUME 24, NUMBER 5 NOVEMBER 1981

Neutron emission in $^{12}C+^{158}Gd$ and $^{13}C+^{157}Gd$ reactions between 8 and 12 MeV/nucleon

A. Gavron,* J. R. Beene, R. L. Ferguson, F. E. Obenshain, F. Plasil, and G. R. Young
Oak Ridge National Laboratory, Oak Ridge, Tennessee 37830

G. A. Petitt
Georgia State University, Atlanta, Georgia 30303

K. Geoffroy Young,† M. Jääskeläinen, and D. G. Sarantites
Washington University, St. Louis, Missouri 63130

C. F. Maguire
Vanderbilt University, Nashville, Tennessee 37235

(Received 15 June 1981)

Neutron spectra in coincidence with evaporation residues and with projectilelike fragments emitted in inelastic scattering reactions have been measured at several bombarding energies for ^{12}C- and ^{13}C-induced reactions leading to the same compound nucleus ^{170}Yb. In the fusion reactions, a nonequilibrium component was observed in the neutron spectra at all beam energies. This component is forward peaked and is associated with a high temperature. The spectra can be parametrized by assuming the nonequilibrium part to result from a hot region ($T \sim 4$ MeV) emitting neutrons isotropically and moving with a velocity of approximately 1 cm/ns. This apparent velocity decreases with decreasing beam velocity. Comparisons are made with predictions based on the generalized critical angular momentum model of incomplete fusion of Siwek-Wilczynska *et al.* No significant difference has been observed between nonequilibrium neutron emission from ^{12}C- and ^{13}C-induced reactions. Neutron emission associated with inelastic scattering reactions cannot be described by simple statistical evaporation from two fragments of equal temperature. Effects which may give rise to the observed energy and angular distributions of neutrons in coincidence with inelastic products are discussed.

[NUCLEAR REACTIONS $^{158}Gd+^{12}C \rightarrow A+n$, $^{157}Gd+^{13}C \rightarrow A+n$, $103 \leq E_{lab} \leq 160$ MeV; $A \equiv$ evaporation residue or projectilelike fragments. $A-n$ coin., $13 \leq \theta_n \leq 141°$, $\theta_A = 18°, 24°$. Neutron multiplicities and energy spectra.]

I. INTRODUCTION

Nonequilibrium emission of light particles resulting from reactions induced with light ions has been studied extensively for a number of years.[1] The first study of nonequilibrium particle emission associated with heavy-ion reactions is that of Britt and Quinton,[2] who measured singles spectra of charged particles and concluded that the fast particles they observed were due to projectile breakup. Recently there has been a great surge of interest in particle emission accompanying heavy-ion-induced reactions, which has resulted in a proliferation of both theoretical and experimental investigations. In most experimental studies the light particles that occur in coincidence either with evaporation residues (ER) (Refs. 3–15) (resulting from fusion or incomplete-fusion reactions) or with inelastic products[16–34] are investigated. While most experiments involve measurements of charged particles, the number of neutron emission studies is also considerable (Refs. 7,15,20,23,24,26,28–30). The main purpose of many investigations has been to establish the existence of nonequilibrium emission in a particular case and to understand its origin by comparing the data with predictions based on one or more theoretical models. In a large number of cases, no conclusive evidence for nonequilibrium emission was found (Refs. 3,4,20,23,24,27–29, 32,33), while in other cases results that were first interpreted in terms of nonequilibrium emission[18] were later shown to be consistent with evaporation from primary reaction products.[32] (For similar changes in interpretation see also Refs. 17 and 34.)

Many theoretical models have been proposed to account for the nonequilibrium emission of fast particles. In addition to the extension of the precompound decay model[1] to heavy-ion-induced reactions,[35,36] theoretical approaches include "hot-spot" models,[37–41] the "piston" model,[42] the promptly emitted particle (PEP) model,[43,44] the Fermi jet model,[45–48] and a number of incomplete-fusion models (Refs. 5,6,8,49–51) (also referred to as massive transfer[6,9,49] and breakup fusion[51] models). In spite of this large number of available models for nonequilibrium emission, direct detailed comparisons between experiment and theory have been sparse. One reason for this gap is the lack of systematic data suitable for comparisons; models have often been applied only to limited data from a single experiment. Thus, no coherent patterns of nonequilibrium particle emission can, as yet, be discerned, and detailed data on nonequilibrium excitation functions, spectra, and angular distributions and on projectile-target and outgoing-channel dependences are needed.

In this work we consider the following two key effects: the energy dependence and onset of nonequilibrium neutron emission (NNE) and the effect of the structure of the projectile. Our study is complementary to a number of earlier related investigations (Refs. 7,10,15,52,53). The energy dependence of NNE associated with evaporation residues has been inferred, for ^{12}C + ^{158}Gd by Sarantites *et al.*[52] and for ^{16}O + ^{154}Sm by Beene *et al.*,[53] from γ-multiplicity data and from the relationship between γ multiplicity and neutron emission, which they measured at one energy. They concluded that partial waves involved in the nonstatistical behavior were predominantly peripheral and that an extended version[15,53] of the generalized critical angular momentum model of incomplete fusion[8,50] can adequately account for the effects they observed. Another important result of earlier investigations concerned the effect of the structure of the projectile. It was found that while NNE was observed for ^{12}C + ^{158}Gd at 152-MeV bombarding energy, it was not observed for ^{20}Ne + ^{150}Nd at 175 MeV, which leads to the same compound nucleus at the same excitation energy.[7] This result is inconsistent with the "sum-rule model" of incomplete fusion of Wilczynski *et al.*,[50] but can be understood in the context of that model if the Q_{gg} systematics of Ref. 50 are replaced by a Q value for the binary projectile fragmentation process.[53]

We present here energy spectra and angular distributions obtained from measurements of neutron emission associated with ER from the ^{12}C + ^{158}Gd and ^{13}C + ^{157}Gd reactions, both of which lead to the ^{170}Yb compound nucleus. Bombarding energies range from 103 to 160 MeV. As mentioned above, these systems were chosen to complement earlier studies. In particular, any effects of structure of the projectile are expected to be especially prominent in comparisons of ^{12}C- and ^{13}C-induced reactions due to the large difference in the neutron separation energies in the projectiles (18.7 MeV in ^{12}C and 4.9 MeV in ^{13}C). Differences in NNE from the two systems were expected, on empirical grounds, due to the observed differences in NNE from ^{12}C- and ^{20}Ne-induced reactions mentioned above[7] and, on theoretical grounds, due to predictions of Boneh *et al.*[47,48] in the framework of a modified Fermi-jet model and to predictions based on the extended incomplete-fusion model.[53]

In addition to results on neutron emission associated with ER, we have also obtained results on neutron emission associated with quasielastic (QE) and with deeply inelastic (DI) reactions. In order to avoid the pitfalls of ambiguous interpretation referred to earlier, we define NNE empirically as neutron emission that cannot be accounted for by statistical evaporation from the fused system (in the case of neutron emission associated with ER) or from fully accelerated projectilelike fragments (PLF) or targetlike fragments (TLF) (in the case of QE and DI reactions). In fusion reactions, NNE spectra are characterized by a high-energy tail and/or by forward peaking in the c.m. system.

Following a description of the experimental method in Sec. II, we present separately, in Secs. III and IV, results and discussion for fusion and fusionlike reactions and, in Secs. V and VI, results and discussion for inelastic reactions. Comparisons with some aspects of the incomplete-fusion model[8,50,53] are made in Sec. IV.

II. EXPERIMENTAL METHOD

The experiments were performed at the Oak Ridge Isochronous Cyclotron with ^{12}C and ^{13}C beams in 4+ and 5+ charge states. Typical

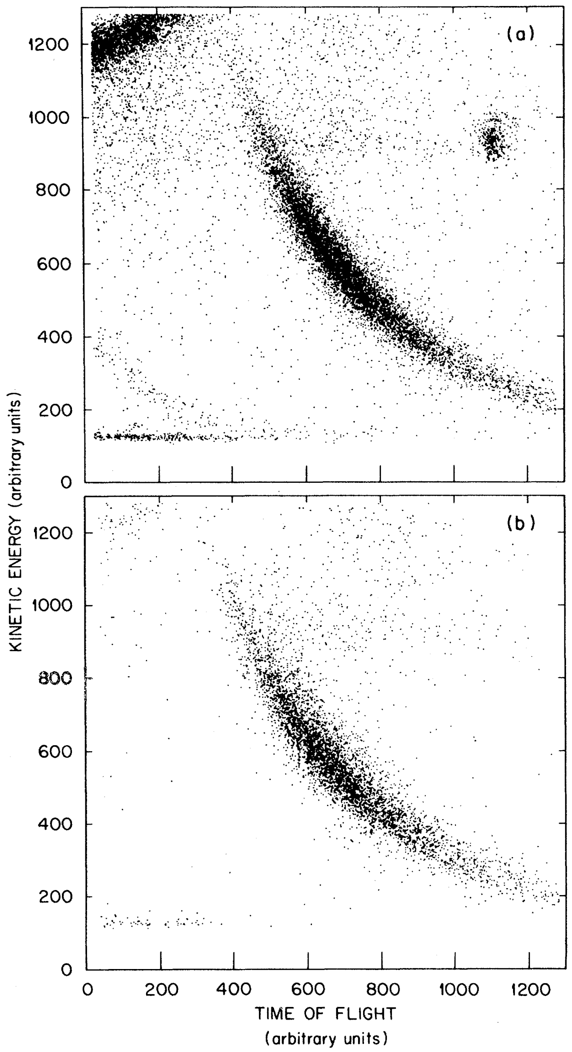

FIG. 1. Scatter plot of evaporation residues as a function of their kinetic energy and time of flight. (a) Singles distribution and (b) events in coincidence with neutrons having energies above 5 MeV.

currents were 1—2 enA. The following beam-energy-target combinations were studied: 150-MeV ^{12}C on ^{158}Gd (1.1 mg/cm^2), 103- and 124-MeV ^{12}C on ^{158}Gd (0.6 mg/cm^2), 140- and 160-MeV ^{13}C on ^{157}Gd (1.1 mg/cm^2), and 110-MeV ^{13}C on ^{157}Gd (0.6 mg/cm^2). The targets were self-supporting, and there was no visible evidence of oxidization or carbon buildup at the end of the experiments.

Neutrons were detected in coincidence with ER and with PLF produced in inelastic reactions. Evaporation residues were detected by two ~24-μm-thick silicon surface barrier detectors positioned at about 7° on each side of the beam axis. Each detector subtended a solid angle of 1.2 msr, and its distance from the target was 18 cm. The ER were identified by their characteristic energy and time of flight with respect to a cyclotron beam pulse. A sample of the data from which this identification was made is presented in Fig. 1(a). A similar plot is presented in Fig. 1(b) for all events in coincidence with neutrons having energies above 5 MeV. The coincidence requirement eliminates a large fraction of random events and other events due to extraneous processes. The higher energy neutrons do not appear to be in coincidence with any particular subset of ER; they result from events with the same distribution of momentum transfers as those of singles events. Typical energies of ER range from 3 to 15 MeV with corresponding flight times of 100—40 ns. Count rates in the Si detectors were approximately 25 kHz, mainly due to elastic scattering. Such events deposit only a small amount of energy in the thin silicon detector and are well separated from ER in time of flight. Dead-time losses were minimized by gating electronically to accept only those events having a flight time to the ER detectors greater than that of elastic scattering events. PLF were detected in a ΔE-E silicon surface barrier telescope with a 33-μm-thick ΔE detector and a 700-μm-thick E detector. Details of its position are given in Table I.

Neutrons were detected in eight NE213 liquid scintillator detectors. Their positions are also presented in Table I. The liquid was encapsulated in aluminum containers (11.8-cm diam) coupled directly to RCA 4522 photomultiplier tubes. The average scintillator thickness was 5.6 cm.

The scattering chamber was spherical with a diameter of 26 cm and was constructed of 3-mm-thick aluminum. At the higher bombarding energies, carbon beams produce high-energy protons that can penetrate the walls of the scattering chamber and produce scintillator pulses similar to those produced by neutrons. Thus, paddles of 1-mm-thick NE102 scintillators, coupled to RCA 8575 photomultiplier tubes, were placed in front of the neutron detectors and used as veto detectors. Protons and other light charged particles were rejected on the basis of their characteristic ΔE and E pulses in the paddle and in the liquid scintillator, respectively.

Neutron time of flight was measured relative to the cyclotron beam pulse with both constant fraction and zero-crossing discriminators. The differ-

TABLE I. Detector positions. Combined results for neutrons in coincidence with evaporation residues are presented in this work for detector combinations $A+H$, $B+G$, $C+F$, and $D+E$.

	Experimental configuration[d]	Neutron detectors							
		A	B	C	D	E	F	G	H
θ[a] (deg)	(1)	126	50	31	13	−18	−34	−63	−101
	(2)	129	61	47	26	−24	−47	−67	−141
γ[b] (deg)	(1)	36	0	0	0	0	0	0	35
	(2)	24	0	0	0	0	0	0	0
Distance[c] (cm)	(1)	56	61	63	66	65	64	56	56
	(2)	51	66	65	63	63	63	61	50

[a] Angle of neutron detector with respect to the beam axis.

[b] Angle of neutron detector above the reaction plane.

[c] Distance of neutron detector from the target.

[d] Runs with the first experimental configuration, group (1) (140-, 160-MeV ^{13}C and 150-MeV ^{12}C) are indicated by (1). Runs with the second configuration, group (2) (103-, 124-MeV ^{12}C and 110-MeV ^{13}C) are indicated by (2). Positions of the ΔE-E telescope were 18° for group (1) runs and 24° for group (2) runs.

ence between these two times provided a measure of the rise time of the scintillator pulses and enabled us to use pulse-shape discrimination to reject gamma rays. Scintillator pulses from subsequent beam bursts (approximately 100 ns later) were also recorded for the purpose of subtracting random coincidences between neutrons and ER or inelastically scattered fragments. The scintillator pulse heights were recorded together with the time information and were subsequently used to determine a constant pulse-height threshold for each neutron detector. This threshold was then used, with the data of Drosg[54] and Anghinofli,[55] in a calculation of the neutron detection efficiency. The neutron detection efficiency was also checked in a 2π geometry with a ^{252}Cf spontaneous-fission neutron source. This method is sensitive to the effects on the efficiency of the presence of the heavy-ion detectors and of the scattering chamber. Adjustments to the calculated efficiencies made on the basis of the ^{252}Cf measurements were less than 15%.

Neutrons with energies below 2 MeV were not included in our analysis for two reasons: (1) small fluctuations in the photomultiplier gain (due to temperature and rate variations) cause large variations in the neutron detection efficiency below 2 MeV; and (2) the neutrons detected at these energies contain a significant contribution from higher energy neutrons that have undergone scattering. (This can be discerned by observing the pulse height as a function of the neutron energy.) These effects do not influence the higher energy portions of the neutron spectra, which are the subject of this investigation. The temporal width of the beam bursts (which determines the resolution of the time-of-flight measurements) varied between 2.5 and 3.0 ns, depending on the beam and its energy. The effect of the time resolution on the shape of the neutron spectra was taken into account in the subsequent analysis.

III. RESULTS — FUSION

Neutron spectra obtained in the eight neutron detectors (in coincidence with evaporation residues) were corrected for detection efficiency and transformed to the c.m. system. Detecting an evaporation residue at a given angle biases the measured spectra and angular distribution; the neutron detection rate on the side of the beam axis opposite to that of the evaporation residue detector is enhanced. This bias was evaluated with a Monte Carlo code which simulates the kinematics of sequential nucleon emission. We found that most of the bias can be removed by averaging, for each neutron detector, multiplicities obtained for neutrons in coincidence with each of the two evaporation residue detectors. A residual effect of this biasing, which causes the neutron multiplicity in our most backward detectors to be enhanced by approximately 10% and to be depleted by a similar amount in our most forward detectors, was taken into account in our analysis. In addition, neutron spectra obtained in neutron detectors at similar angles on opposite sides of the beam axis were averaged to improve the statistics. This averaging was also taken into account in the Monte Carlo calculations used in the data analysis procedure.

Experimental neutron spectra expressed as $4\pi\, d^2N/dE\, d\Omega$, in units of neutrons/MeV, are presented in Figs. 2–4 for the six beam-energy-projectile combinations. Neutron spectra from ^{12}C- and ^{13}C-induced reactions are superimposed for similar values of beam energy per nucleon. The spectra are presented for four average angles of the neutron detectors and averaged over the two evaporation residue detectors for reasons given above. In general, the neutron spectra exhibit the features described by Westerberg *et al.*,[7] including an excess of high-energy neutrons. This high-energy tail is more pronounced in the forward direction than in the backward direction. There is no obvious difference between neutron spectra obtained from ^{12}C-induced reactions and those obtained from ^{13}C-induced reactions at similar bombarding energies per nucleon. (The minor differences evident in Fig. 3 can be attributed to the slightly different experimental configurations in the two reactions; see Table I.)

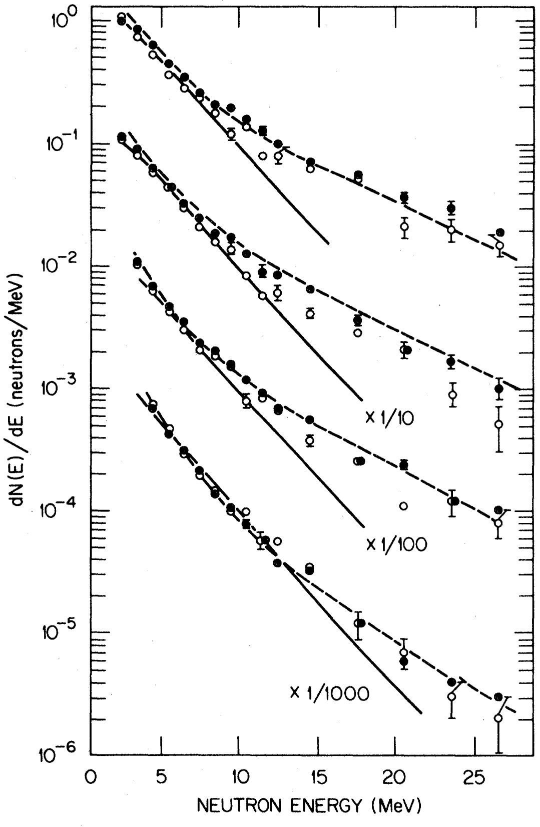

FIG. 2. Spectra of neutrons in coincidence with evaporation residues. Open circles: ^{12}C + ^{158}Gd (150 MeV); closed circles: ^{13}C + ^{157}Gd (160 MeV); angular combinations (from top to bottom): $D+E$, $C+F$, $B+G$, $A+H$ (see Table I). The solid line is obtained after fitting the ^{12}C data using Eq. (1) (see text, Sec. III A). The dashed line is obtained after fitting the ^{13}C data using the two-source model (see text, Sec. III B).

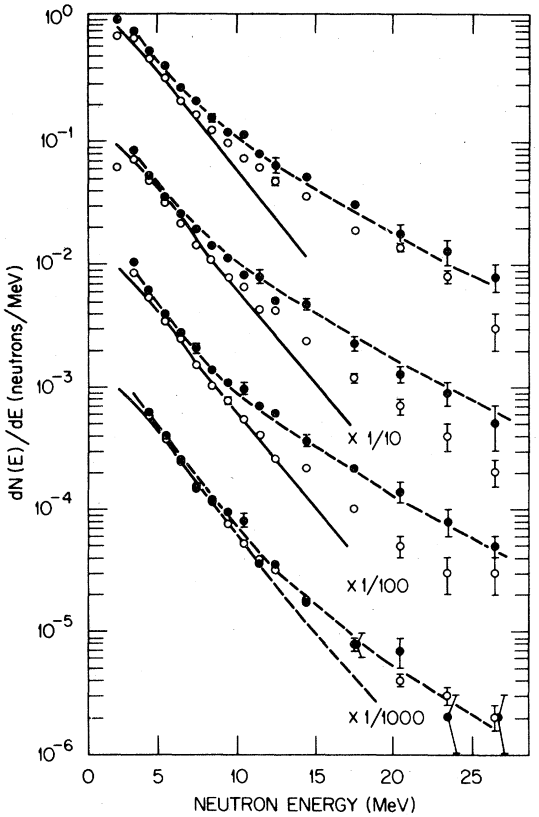

FIG. 3. Similar to Fig. 2, but for ^{12}C at 124 MeV (open circles) and ^{13}C at 140 MeV (closed circles). Note (see Table I) that the experimental configuration is slightly different in the two cases.

Determination of the nonequilibrium part of the neutron spectrum involves subtraction of the equilibrium part of the spectrum. Since there is no uniquely defined procedure for doing this, we have

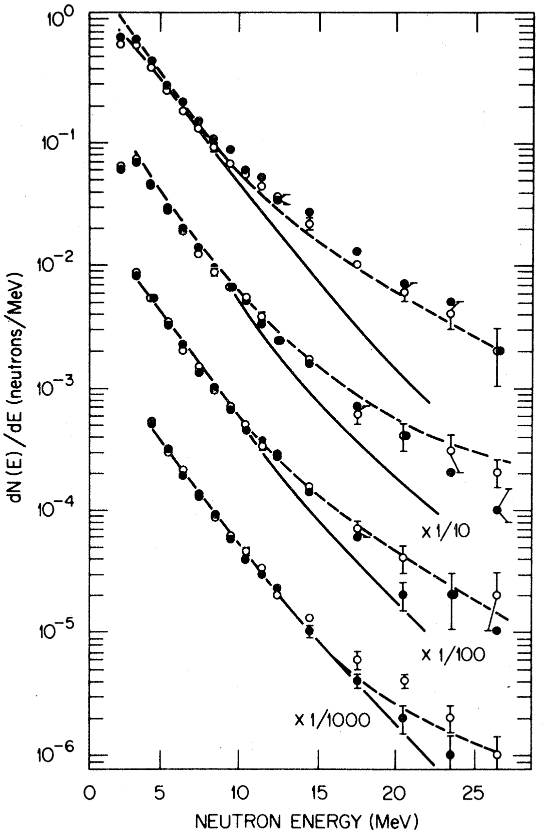

FIG. 4. Similar to Fig. 2, but for ^{12}C at 103 MeV (open circles) and ^{13}C at 110 MeV (closed circles).

chosen to proceed by means of two different methods, which should provide upper and lower estimates of the amount of NNE.

A. Lower limit estimate of NNE

In this method we fit each neutron spectrum up to a c.m. neutron energy of 9 MeV by assuming the neutrons were produced entirely by evaporation. However, the nonequilibrium tail, which is prominent above 9 MeV, also extends down to energies below this value. Therefore, this fit maximized the contribution of evaporated neutrons to the total multiplicity, thus providing a lower limit for the NNE multiplicity. The shape of the evaporated neutron spectrum $\phi(\epsilon)$ was chosen to be

$$\phi(\epsilon)=\epsilon^{0.6}\exp[-\epsilon/T] , \tag{1}$$

where ϵ is the neutron c.m. energy and T is the nuclear temperature. This spectrum conforms to results of evaporation calculations for the ^{170}Yb compound nucleus in this energy and angular momentum range.[56] Effects of the finite time-of-flight resolution and of spectrum biasing due to the detection of an evaporation residue have been taken into account. Both the temperature and normalization were varied, and the least-squares method was used to obtain a best fit of the calculated spectra to the experimental results at the four angles. The NNE multiplicity at each angle was then taken to be the difference between the integrated experimental neutron spectrum and the multiplicity obtained by integrating Eq. (1) for $\epsilon > 8$ MeV.

Temperatures and multiplicities obtained by this fitting procedure are presented in Table II. The calculated spectra are shown for the ^{12}C case in Figs. 2–4 (full lines). The temperatures obtained here are similar to those presented in Ref. 7 for ^{20}Ne + ^{150}Nd reactions leading to the same compound nucleus at similar angular momentum and excitation energy. In that reaction, no evidence was found for NNE, which made it possible to determine a unique value of the temperature. Angle-integrated values for the lower limit on

TABLE II. Lower limit estimates of NNE multiplicities (see text, Sec. III A).

Reaction	T_{Eq}[a] (MeV)	$\bar{M}_{Eq}$[b]	M_{NE}[c]$(A+H)$[d]	M_{NE}[c]$(B+G)$[d]	M_{NE}[c]$(C+F)$[d]	M_{NE}[c]$(D+E)$[d]	$\bar{M}_{NE}$[e]
160-MeV ^{13}C	2.4	7.0	−0.05 ± 0.02	0.39 ± 0.03	0.47 ± 0.03	0.85 ± 0.03	0.21 ± 0.02
140-MeV ^{13}C	2.2	6.3	0.02 ± 0.01	0.28 ± 0.02	0.29 ± 0.03	0.48 ± 0.01	0.14 ± 0.01
110-MeV ^{13}C	2.0	5.9	0.00 ± 0.01	0.05 ± 0.01	0.06 ± 0.01	0.22 ± 0.01	0.05 ± 0.01
150-MeV ^{12}C	2.3	7.1	0.08 ± 0.03	0.31 ± 0.03	0.27 ± 0.04	0.62 ± 0.05	0.16 ± 0.01
124-MeV ^{12}C	2.1	6.5	0.06 ± 0.01	0.07 ± 0.01	0.12 ± 0.01	0.32 ± 0.05	0.08 ± 0.01
103-MeV ^{12}C	2.0	5.8	0.05 ± 0.01	0.08 ± 0.01	0.01 ± 0.01	0.16 ± 0.01	0.06 ± 0.01

[a] T_{Eq} is obtained by fitting the data from 4 to 9 MeV using Eq. (1).

[b] $\bar{M}_{Eq}$ is obtained from the normalization of $\phi_{Eq}(\epsilon)$, given in Eq. (1), to the experimental data.

[c] $M_{NE}(\theta)=\sum_{\epsilon=8}^{\infty}N_{\exp}(\epsilon)-\int_{8}^{\infty}\phi_{Eq}(\epsilon)d\epsilon$ (neutrons/4π sr).

[d] The letters in the parentheses next to multiplicity symbols indicate detector combinations (see Table I).

[e] $\bar{M}_{NE}$ is obtained by integrating $M_{NE}(\theta)$.

NNE range from 0.21±0.02 neutrons for 160-MeV ^{13}C to 0.05±0.01 neutrons for 110-MeV ^{13}C.

B. Upper limit estimate of NNE

An alternative method for fitting the data is to assume arbitrarily that, in addition to the evaporation spectrum [Eq. (1)], there exists another source of neutrons which moves with a velocity larger than that of the c.m. (to account for the forward peaking) and which may have a different temperature. We assumed this source to have a spectrum $\phi_{\rm NE}(\epsilon)$ given by

$$\phi_{\rm NE}(\epsilon)=\epsilon\exp[-\epsilon/T_{\rm NE}]\ . \tag{2}$$

A least-squares fit of the calulated neutron spectra to the experimental data at the four average angles (Table I) has been obtained for each beam-energy-projectile combination by varying the following parameters: (i) the relative multiplicities of the evaporation and nonequilibrium sources, (ii) the temperatures $T_{\rm Eq}$ and $T_{\rm NE}$ of the two sources, and (iii) the velocity $V_{\rm NE}$ of the nonequilibrium source. Effects of the finite resolution in the neutron time of flight and of multiplicity biasing due to evaporation residue detection were also taken into account in these calculations. The parameters which minimize the sum of the square of differences between the calculated spectra and the experimental results are presented in Table III. The dashed lines in Figs. 2–4 indicate spectra calculated with the parameters obtained from fits to the ^{13}C data. We note that these calculated spectra provide a good description of the experimental results. We can compare the total neutron multiplicities obtained here to those obtained from individual *xn*, *xnα*, and *xnp* cross section measurements. With 124-MeV ^{12}C we obtained a total of 7.2 neutrons, and averaging the individual cross sections of Ref. 52 for this case, we also obtain 7.2 neutrons. At 150 MeV we obtain 8.2 neutrons compared to 8.5 calculated from data of Ref. 52. Thus despite the fact that our overall normalization is highly model dependent (30–50% of the evaporated neutrons are below our threshold energy), this procedure provides total neutron multiplicity in close agreement with values found by different methods in Ref. 52. This agreement supports the point of view that the multiplicity values of Table III are more nearly correct that those of Table II and that, therefore, the lower limit method used to obtain the nonequilibrium neutron multiplicity values of Table II results in underestimates of NNE. In the context of this two-source analysis the nonequilibrium source is responsible for 18% of the total neutron multiplicity at the highest excitation energies and for 6% at the lowest. Temperatures obtained for the equilibrium components are approxi-

TABLE III. Upper limit estimate of NNE (see text, Sec. III B).

Reaction	$T_{\rm Eq}$[a] (MeV)	$T_{\rm NE}$[b] (MeV)	$V_{\rm c.m.}$[c] (cm/ns)	V_B[d] (cm/ns)	$V_{\rm NE}$[e] (cm/ns)	$\bar{M}_{\rm Eq}$[f]	$\bar{M}_{\rm NE}$[g]
160-MeV ^{13}C	1.60	4.2	0.40	3.98	1.2	7.0	1.5
140-MeV ^{13}C	1.54	3.8	0.35	3.58	1.0	6.3	1.1
110-MeV ^{13}C	1.60	3.7	0.31	2.89	0.8	5.9	0.4
150-MeV ^{12}C	1.63	4.2	0.35	3.94	0.9	7.1	1.1
124-MeV ^{12}C	1.57	4.0	0.32	3.36	0.8	6.5	0.7
103-MeV ^{12}C	1.59	4.1	0.29	2.84	0.7	5.8	0.4
Error[h] in parameter	0.03	0.1			0.1	0.2	0.1

[a] Temperature parameter in Eq. (1).

[b] Temperature parameter in Eq. (2).

[c] c.m. velocity (provided for reference).

[d] Velocity of projectile corresponding to its energy in excess of the Coulomb barrier (provided for reference).

[e] Velocity of moving NNE source.

[f] Equilibrium neutron emission multiplicity.

[g] NNE multiplicity.

[h] The assigned errors are the variation in the parameters that cause an increase of approximately 10% in chi square.

mately 1.6 MeV in all cases. This is significantly lower than the values of 1.9–2.2 MeV quoted in Ref. 7 for ^{20}Ne+^{150}Nd, but similar to values obtained by a two-component method for ^{16}O +^{154}Sm.[15] Statistical model calculations[56] (at excitation energies remaining after NNE) predict temperatures of the order of 2.3–2.6 MeV, and it is therefore possible that the nonequilibrium spectrum defined in Eq. (2) leads to an overestimate at low neutron energies. However, the sum of the two neutron sources [Eqs. (1) and (2)] provides a reasonable description of all the measured spectra and angular distributions, even though the decomposition into the two components may not be reliable in the intermediate energy range. Furthermore, the velocities and temperatures of the second component are determined mainly by the high-energy tails and are not substantially affected by possible systematic errors in the lower energy part of $\phi_{NE}(\epsilon)$.

C. Onset of NNE

We present in Fig. 5 the nonequilibrium neutron multiplicities obtained by two methods of analysis described above. There is a large difference between the lower and upper limits. It is therefore essential that various theories be tested directly against the experimental spectra at each angle, with evaporation neutrons included in the calculated spectra. However, both methods enable us to make an extrapolation of the amount of NNE vs excitation energy, and both methods lead to the conclusion that the onset of nonequilibrium emission is in the vicinity of 80-MeV excitation energy (~90-MeV beam energy) for both ^{12}C and ^{13}C projectiles.

An additional parameter R, which can be used as a measure of the amount of NNE and which is model independent, is defined as

$$R=\int_{14}^{\infty}N(\epsilon)d\epsilon\Big/\int_{4}^{7}N(\epsilon)d\epsilon\ , \tag{3}$$

where $N(\epsilon)$ is the (experimental) c.m. neutron spectrum. The integration limits were chosen for the following reasons: above 14 MeV the spectrum results mainly from high-energy NNE; between 4 and 7 MeV the spectrum is dominated by the evaporation component. Energies below 4 MeV are excluded because of the sensitivity of the spectra in this range to pulse-height threshold shifts.

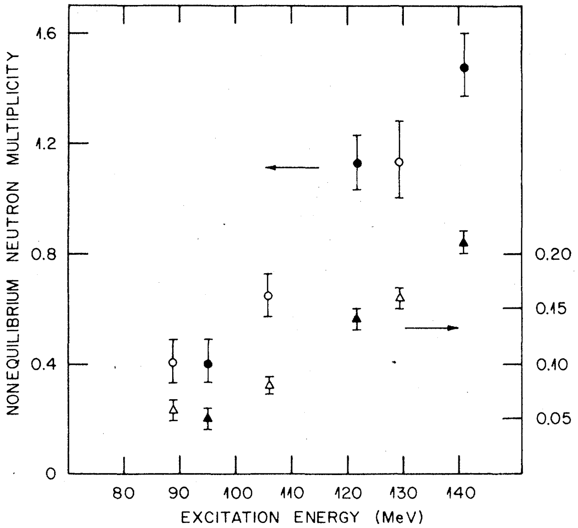

FIG. 5. Upper and lower limits of NNE multiplicity as function of excitation energy (see text). ^{13}C-induced reactions are indicated by closed symbols and ^{12}C-induced reactions by open symbols. The circles represent the upper limit values discussed in Sec. III B, and the triangles represent lower limit values of Sec. III A. The left-hand scale applies to the circles and the right-hand scale to the triangles.

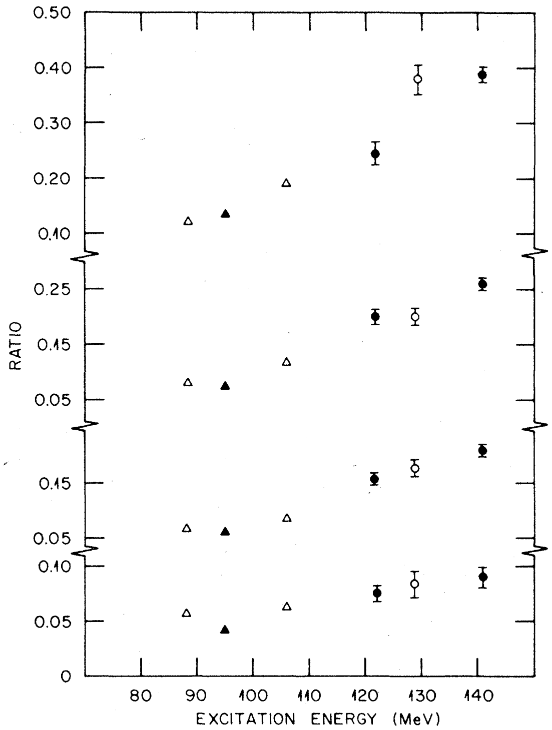

FIG. 6. Ratio of fast to slow neutrons [Eq. (3)] as a function of excitation energy. Closed symbols represent ^{13}C reactions and open symbols ^{12}C reactions. Circles depict the first experimental configuration [group (1) of Table I] and triangles the second configuration [group (2) of Table I]. Detector combinations involved, from top to bottom, are $D+E$, $C+F$, $B+G$, and $A+H$ (see Table I).

Values of R for different projectile energies and neutron detection angles are presented in Fig. 6. The general features of NNE are again evident: an increase with increasing beam energy and with decreasing detection angle.

IV. DISCUSSION — NNE ASSOCIATED WITH ER

A. Critical angular momentum and incomplete fusion

The generalized critical angular momentum model of incomplete fusion,[8] and extensions of the model,[15,50,53] will be used in this section in comparisons between experiment and theory. The model and its implications have been discussed in detail elsewhere (Refs. 8,10,13,15,50,53), and only a summary is presented here. In its present stage of development, the extended model has successfully explained available information on multiplicity saturation for (HI,xn) reactions and on NNE associated with various xn channels.[15]

The basic assumption of the model[8] is that fusion takes place for entrance-channel orbital angular momenta from zero to a critical value. The model gives a specific prescription for estimating this critical value. For partial waves beyond the critical value, fusion may occur if a portion of the projectile escapes, carrying with it a fraction of the initial angular momentum. The rest of the projectile is then assumed to fuse with the target nucleus, provided that the remaining angular momentum is less than the critical angular momentum for the incomplete system. It is further assumed that the fraction of angular momentum carried away is given by the ratio of the mass of the emitted fragment to the mass of the projectile and that fusion with the largest possible fragment is favored. These assumptions result in a hierarchy of partial fusion reactions (and accompanying fast particle emission), each localized in a particular region of angular momentum space. Similar ingredients and assumptions are contained in quantum-mechanical approaches.[49,51] Alternative names for incomplete fusion, such as "massive transfer"[6,9] and "breakup fusion,"[51] have also been used.

To allow for the competition between various possible incomplete-fusion channels, Wilczynski *et al.*[50] have applied a "sum-rule" formalism to fusion and incomplete-fusion reactions. It is assumed in this approach that the individual reaction probabilities are scaled by the available phase space and that they are additionally constrained by the entrance-channel angular momentum limitations discussed above.

For the purpose of subsequent discussion we give below the expression for $P(i)$, which defines the phase space factors used to give weight to the various possible final channels:

$$P(i)=\exp[Q_{gg}(i)-Q_c(i)]/T \ , \tag{4}$$

where Q_{gg} is the ground-state Q value for the process i, $Q_c=q_c e^2(Z'_1Z'_2-Z_1Z_2)$, T and q_c are adjustable constants, and Z' and Z refer to nuclear charges in the entrance and exit channels, respectively. The quantity $P(i)$ thus accounts for the competition between various channels i, except for an angular momentum term (spin cutoff factor) which is included in the theory separately. In Ref. 50, T was taken to be 3 MeV.

B. Effects of projectile structure

One of the main motivations in undertaking the present study was to investigate effects of projectile structure on NNE. As was pointed out in the Introduction, differences in NNE from ^{12}C and ^{13}C reactions were expected on both experimental and theoretical grounds. The observation that NNE accompanies fusion reactions between ^{12}C and ^{158}Gd but not between ^{20}Ne and ^{150}Nd suggests that structure effects may be important, since both reactions lead to the same compound nucleus ^{170}Yb at the same excitation energy. In addition, NNE is observed from fusion reactions between ^{16}O and ^{154}Sm (again leading to ^{170}Yb) but to a smaller extent than in the ^{12}C + ^{158}Gd case.[15,53] Theoretical support for the idea that projectile structure may play a role in NNE is provided by the modified Fermi-jet model of Boneh *et al.*,[47,48] which specifically predicts a large difference in NNE between ^{12}C- and ^{13}C-induced reactions. From the results presented in the previous section it is clear that, whatever structure effects may play a role in NNE, the large difference in the binding energy of the last neutron between ^{12}C and ^{13}C does not result in an observable effect, and that the model of Boneh *et al.* is not valid.

It should be pointed out that the observed differences in NNE between ^{12}C- and ^{20}Ne-induced reactions may be attributed simply to the difference in the energy per nucleon (above the Coulomb barrier) between the two cases. In Ref. 7 this energy was considerably higher in the ^{12}C + ^{158}Gd case than in the ^{20}Ne+ ^{150}Nd case. The energy per nucleon in the case of 175-MeV ^{20}Ne+^{150}Nd is similar to those of the lowest bombarding energies involved in this work. From Table III it can be seen that in the cases of 110-MeV ^{13}C+^{157}Gd and 103-MeV ^{12}C+^{158}Gd the average NNE multiplicity, $\bar{M}_{\rm NE}$, is only 0.4. Such a low value of $\bar{M}_{\rm NE}$ probably would have remained undetected in the less sensitive measurements of Ref. 7. Preliminary results from a recent experiment,[61] in which the present study was extended to the case of 176-MeV ^{20}Ne+^{150}Nd, indicate that the value of $\bar{M}_{\rm NE}$, based on a two-source analysis, is, in fact, 0.4.

Recently, results from investigations of NNE associated with fusion and fusionlike products for the ^{16}O+^{154}Sm reaction[15,53] were interpreted on the basis of the generalized critical angular momentum model of incomplete fusion outlined above.[8,50] Agreement between experiment and theory was very good in many aspects, but not in those involving the structure of the projectile.[53] In order to remedy the perceived deficiencies of the Wilcynski sum-rule model,[50] Beene *et al.*[53] have replaced the Q_{gg} values of Eq. (4) with Q values appropriate for projectile fragmentation processes, i.e., with the separation energies for specific channels involved. This modification of the incomplete-fusion model resulted in a reasonable description of the differences in NNE observed in ^{12}C-, ^{16}O-, and ^{20}Ne-induced reactions.

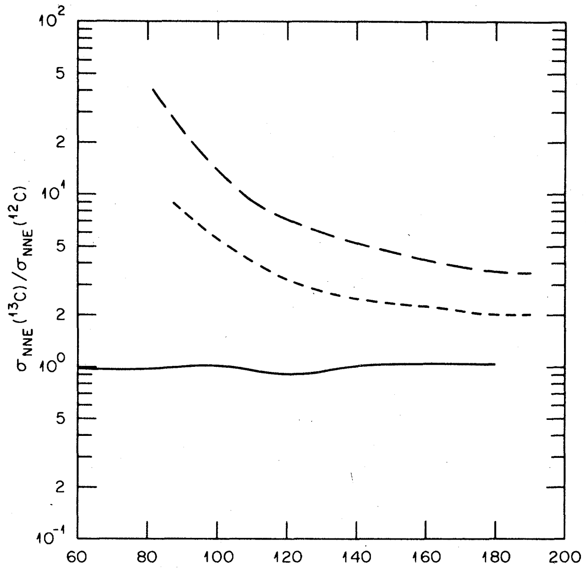

FIG. 7. Calculated ratio of NNE associated with ER for ^{13}C-induced reactions to NNE for ^{12}C-induced reactions. The solid curve is from the model of Wilczynski *et al.* (Ref. 50). The dashed curves are from a modified version of the model. (Ref. 53). The long-dash curve is for $K=4$, and the short-dash curve is for $K=8$ (see text, Sec. IV B).

In Fig. 7 the solid curve indicates the predicted ratio of NNE from the ^{13}C+^{157}Gd reaction to the NNE from the ^{12}C+^{158}Gd reaction. The prediction was made with the unaltered sum-rule model of Ref. 50 and the parameters suggested in that work. Since the predicted ratio is close to unity and since we observe no significant difference between ^{12}C- and ^{13}C-induced reactions (see Figs. 2−6), we conclude that the agreement between experiment and theory is, in this respect, excellent.

Predictions based on the modifications of the Wilczynski model discussed in Ref. 53 are also shown in Fig. 7 for two values of a parameter K defined by $T^2=K\epsilon$, where T is the parameter of Eq. (4) and ϵ is the relative energy per nucleon above the Coulomb barrier. As mentioned above, the ground-state Q value for our case, Q_{gg} of Eq. (4), was replaced by the neutron separation energy of the projectile. One of the two values of K used in Fig. 7, $K=8$, corresponds to the extreme case of the conversion of all of the kinetic energy into projectile excitation. From Fig. 7 it can be seen that this modification of the partial fusion model results in a disagreement between experiment and theory in our case. The reason Q_{gg} values appear to be appropriate for our case and for the case of Ref. 50, while projectile fragmentation Q values seem to be appropriate for the studies of Refs. 7, 15, and 53, is not understood.

C. NNE multiplicities

In view of the fact that a unique prescription for the decomposition of our results into NNE and evaporation does not exist, we must be content with upper and lower limits for NNE multiplicities. It is instructive, however, to compare these limits with theoretical predictions. In Fig. 8 a comparison of measured multiplicities with the Wilczynski sum-rule model[50] is shown as a function of bombarding energy. Our upper and lower limits bracket the theoretical prediction, although the predicted flattening of the NNE multiplicity curve with increasing bombarding energy is not observed.

D. Velocities and temperatures of the NNE sources

In the previous section it was shown that our results can be adequately parametrized by consider-

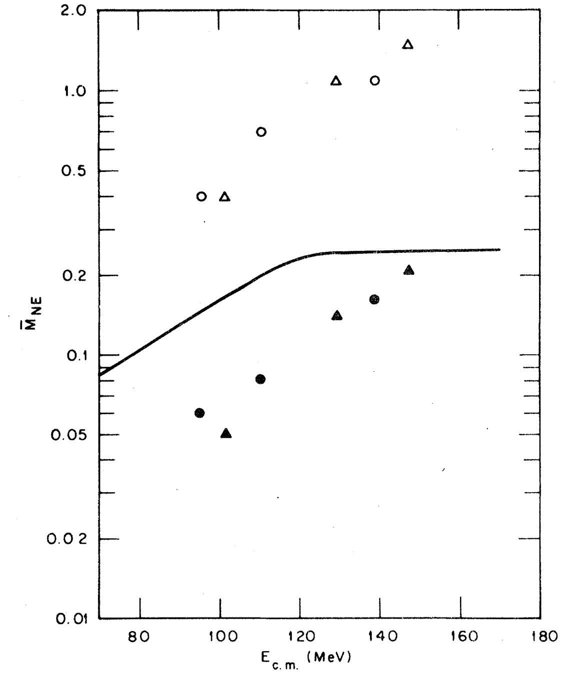

FIG. 8. Average nonequilibrium neutron multiplicities. The curve was obtained from the Wilczynski *et al.* (Ref. 50) sum-rule model. The open symbols refer to values from Table III and the closed symbols to values from Table II. Triangles are for $^{13}C+^{157}Gd$ and circles for $^{12}C+^{158}Gd$.

ing emission from two sources: the equilibrated compound nucleus and an NNE source with properties given in Table III. While we must caution against inferring that such parametrizations necessarily describe actual mechanisms, it is nevertheless interesting to speculate about the meaning of the parameters involved, such as the velocities and temperatures of the NNE sources.

It can be noted from Table III that the velocity of the NNE source, V_{NE}, is intermediate between the velocity of the center of mass $V_{c.m.}$ and the velocity of the projectile just prior to interaction V_B, i.e., the velocity corresponding to the beam energy in excess of the Coulomb barrier. The range of the ratio V_{NE}/V_B in Table III varies from 0.23 to 0.3. The ratios obtained in Ref. 53 by a similar treatment for $^{16}O+^{154}Sm$ were in the vicinity of 0.4. This relatively low value of V_{NE}/V_B was explained on the basis of a classical orbiting model.[53] We have applied a similar approach to our results.

We estimated the tangential velocity of the projectile, V_T, from a classical Rutherford orbit. The orbital angular momentum considered to be appropriate for our purpose is the average orbital angular momentum (at a given bombarding energy) corresponding to all NNE processes, as given by the sum-rule model of Ref. 50. The separation distance was taken to be $1.2(A_p^{1/3}+A_T^{1/3})$ fm, where A_p and A_T are the mass numbers of the projectile and the target, respectively. The velocities V_B and V_T are shown in Fig. 9 as a function of the c.m. bombarding energy. Also shown in Fig. 9 are the projection of the tangential velocity on the beam axis $|\vec{V}_T \cdot \hat{K}_B|$ and the experimental results. It is clear that the NNE source velocity obtained from our data is approximately a factor of 2 lower than the projection of V_T on the beam direction. On the other hand, the observed gradual increase of V_{NE} with increasing bombarding energy is similar to the increase in the tangential velocity. If we had allowed for the transfer of a certain amount of orbital angular momentum into internal angular momentum (i.e., for "tangential friction"), the projection $|\vec{V}_T \cdot \hat{K}_B|$ could have been brought into agreement with the observed source velocity. For the limiting case of the sticking condition, $|\vec{V}_T \cdot \hat{K}_B|$ is, in fact, estimated to be lower than the observed source velocity. While tangential friction may indeed play a role, it contradicts a basic assumption of the model of Refs. 8 and 50, which implicitly assumes that the only way relative angular momentum is dissipated, at least in the early stages of the reaction, is by the emission of particles or of fragments of the projectile.

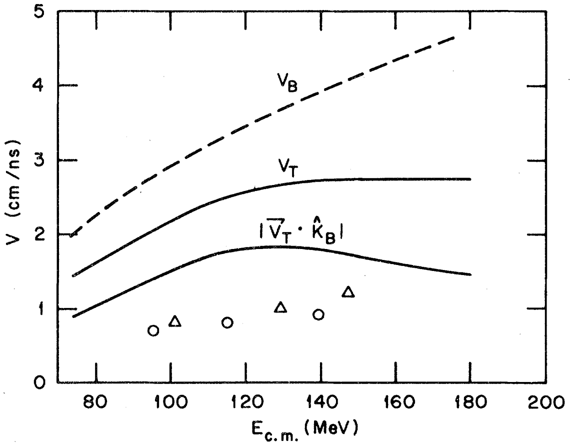

FIG. 9. Velocity as a function of c.m. bombarding energy. V_B (dashed curve) is the velocity of the projectile corresponding to its energy above the Coulomb barrier. V_T is the tangential velocity of the projectile at the time of interaction (see text), and $|\vec{V}_T \cdot \hat{K}_B|$ is the projection of V_T on the beam direction. The data points are the velocities of the nonequilibrium source from Table III. Triangles refer to ^{13}C reactions and circles to ^{12}C reactions.

In Table III it is shown that the temperature of the NNE source, T_{NE}, remains constant at a value near 4 MeV. In contrast to the situation regarding the velocity of the NNE source, we find that a value of about 4 MeV for T_{NE} is reasonable in the context of our picture, but that the failure of T_{NE} to increase with increasing bombarding energy is difficult to understand. Using the Rutherford orbit description given above, we can deduce an upper limit of T_{NE} values if we assume that, at the separation distance given above, the radial kinetic energy is instantly converted to excitation energy E^* of the projectilelike fragment. This excited fragment would then constitute the NNE source. If we relate E^* to T_{NE} by $E^* = aT^2$ and use $a = A/8$ and $A = 12$, we obtain the solid curve of Fig. 10. Also shown in the figure are T_{NE} values deduced from our experimental results, as well as a temperature estimate of Bertsch as reported by Awes *et al.*[57] It can be seen that, while our T_{NE} values are of similar magnitude to those of the calculated curves, we do not observe the predicted increase in T_{NE} with bombarding energy.

E. Comparison with the precompound decay model

The precompound model has been very successful in interpreting nonequilibrium emission resulting from reactions with light ions.[1] The extension of this model to heavy-ion-induced reactions is being developed by Blann.[35,36] Application to heavy-ion reactions is complicated by several effects.[36] For example, since the coalescence period of the target and projectile nuclei is comparable to nucleon-nucleon collision periods, particle emission probably takes place during the coalescence process. In addition, the assumption that intrinsic excitations are the only degrees of freedom that need to be considered may not be valid due to the possibility of exciting collective degrees of freedom. In order to deal with some of these complications, Blann[58] has adapted an approach referred to as the modified Boltzmann master equation (BME) model. In this model a term has been added to allow for the time-dependent addition of nucleons from the projectile to the coalescing system. The key parameters in the model are the initial exciton number and transition probabilities (taken from free nucleon-nucleon scattering cross sections) for nucleons to scatter from an initial to a final state.

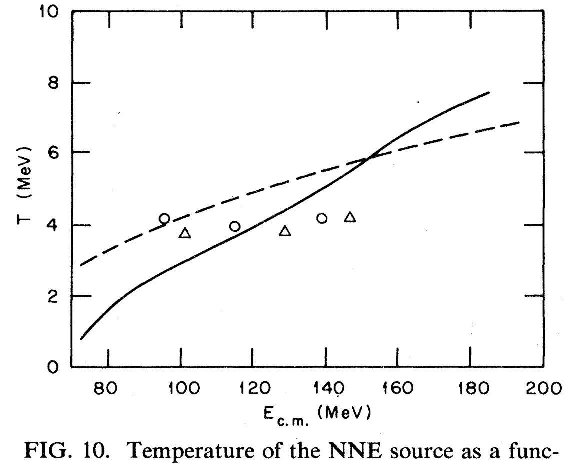

FIG. 10. Temperature of the NNE source as a function of the c.m. bombarding energy. The data points are from Table III, with triangles referring to ^{13}C-induced reactions and circles referring to ^{12}C-induced reactions. The dashed curve was obtained from Ref. 57. The solid curve is from a classical orbit picture combined with the Wilczynski *et al.* sum-rule model (Ref. 50) (see text).

Blann has provided us with calculated spectra for our cases, which we used to make direct comparisons between the BME model and experimental results.[58] Our two-source parametrization discussed in Sec. III is characterized by an NNE source temperature of about 5 MeV for all systems, provided only neutron c.m. energies greater than 10 MeV are considered. In contrast, the BME model, assuming an initial exciton number equal to the number of particles in the projectile, predicts temperatures of 9 MeV for 150-MeV $^{12}C + ^{158}Gd$ and 7 MeV for 120-MeV $^{12}C + ^{158}Gd$.

We further compared the empirical ratios R, defined in Eq. (3), with the same ratios deduced from a combination of the BME model[58] and a compound nucleus deexcitation calculation[56] (from which we obtained the low-energy portion of the spectrum). The calculated values of R are 0.074 for the 160-MeV ^{13}C case, 0.062 for 140-MeV ^{13}C, 0.062 for the 150-MeV ^{12}C case, and 0.053 for the 120-MeV ^{12}C case. The corresponding values obtained from our data are 0.154, 0.104, 0.110, and 0.068. (This last value of R is for 124-MeV ^{12}C rather than 120 MeV.) Thus the high-energy component of the experimental neutron spectra increases much more rapidly (relative to the low-energy component) than is predicted by the BME model.

The above discrepancies between the BME model and the experimental results must be viewed with caution, since they may only indicate that better choices of initial parameters and/or model assumptions need to be made. For example, the initial exciton number, which influences the predicted NNE temperature, should be regarded as a lower limit since it does not take into account either collective excitations or the exchange of nucleons between target and projectile. An increase in the intitial exciton number would lead to lower temperatures and thus to better agreement between experiment and theory. Furthermore, the transition probabilities are very sensitive to the assumed nuclear density in the overlap (neck) region of the coalescing nuclei. A value equal to the average density of nuclear matter was used in the calculations, but the density may, in fact, be as low as half this value. A lower assumed density would result in calculated values of R in better agreement with experiment. Finally, the BME model has thus far been developed only for zero angular momentum, while evidence from γ-multiplicity measurements and the success of the partial-fusion model in explaining our results both indicate that NNE is associated with high partial waves.[52,53] More systematic comparisons between experiment and the BME model are needed before a verdict can be reached on the usefulness of the model.

F. Comparisons with other models

In the absence of other model calculations made specifically for the systems under investigation, it is hazardous to draw conclusions with regard to the validity of any particular model. On the basis of the successful parametrization of our results in terms of two emission sources, as presented in Sec. III, we might conclude that the general category of "hot-spot" models[37–41] should be applicable to our cases. The hot-spot model of Garpman *et al.*[40] has had some success in explaining the data from the $^{16}O+^{154}Sm$ reaction.[15] Our results are in many ways similar to those of Ref. 15, and we can expect that this version of the hot-spot model would also be successful if it were applied to our cases. One interesting aspect of this approach is that significant differences are expected between neutron and proton emission. For the $^{16}O+^{93}Nb$ reaction, charged-particle emission data,[59] together with earlier neutron emission data,[26] may provide a more stringent test of this theory.

With regard to the PEP model of Bondorf *et al.*,[43,44] limited comparisons have been made in the $^{16}O+^{154}Sm$ case with inconclusive results.[15] One feature of this model which is in apparent disagreement with our results and those of Ref. 15 is the prediction that nonequilibrium neutrons with energies above 14 MeV are expected to be emitted only in the forward direction. We find, in fact, a significant number of them at backward directions, as can be seen in Figs. 2–4.

V. RESULTS — INELASTIC COLLISIONS

Measurements of neutron spectra in coincidence with the PLF in inelastic reactions can be divided into two groups based on the two experimental configurations we have used (see Table I): (1) the higher energy group, consisting of 140- and 160-MeV ^{13}C- and 150-MeV ^{12}C-induced reactions, and (2) the lower energy group, consisting of 103- and 124-MeV ^{12}C- and 110-MeV ^{13}C-induced reactions. In group (1), the PLF kinetic energy spectrum exhibits a QE peak and, in addition, a more strongly damped DI component. An example of such a spectrum is shown in Fig. 11. The PLF kinetic energy spectrum is presented for $Z=6$ in the 150-MeV ^{12}C reaction (closed points). In group (2), only a quasielastic peak is evident; a typical spectrum for $Z=6$ fragments is shown in Fig. 12 (closed points). The spectrum of fragments in coincidence with all neutrons having laboratory energies above 2 MeV (detected in any of the eight detectors) is indicated by open points in the two figures. For energy losses greater than 20 MeV,

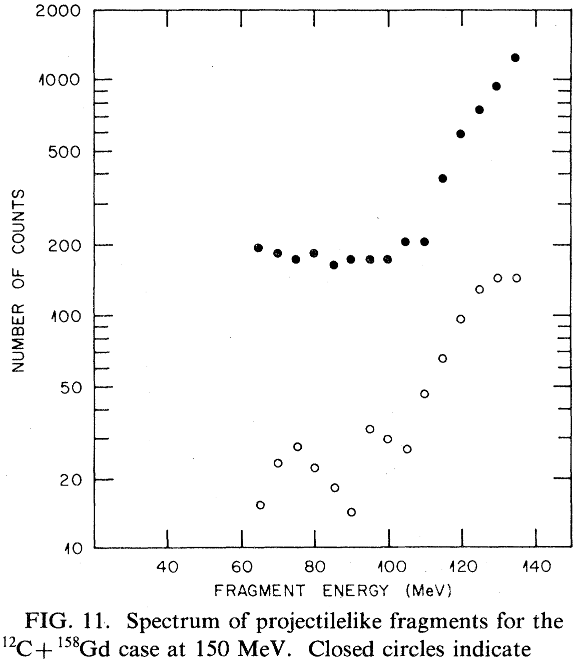

FIG. 11. Spectrum of projectilelike fragments for the $^{12}C+^{158}Gd$ case at 150 MeV. Closed circles indicate scaled-down singles events, and open circles show the total number of events with coincident neutrons.

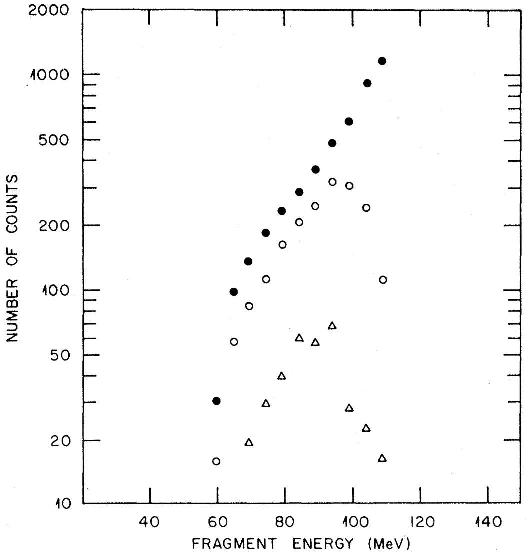

FIG. 12. Same as Fig. 11, but for ^{13}C+^{157}Gd at 110 MeV. The triangles indicate the number of events in coincidence with neutrons between 4 and 9 MeV observed in detector *D*.

the ratio of neutron coincidence events to PLF singles is approximately constant, indicating a flattening of the total neutron multiplicity.

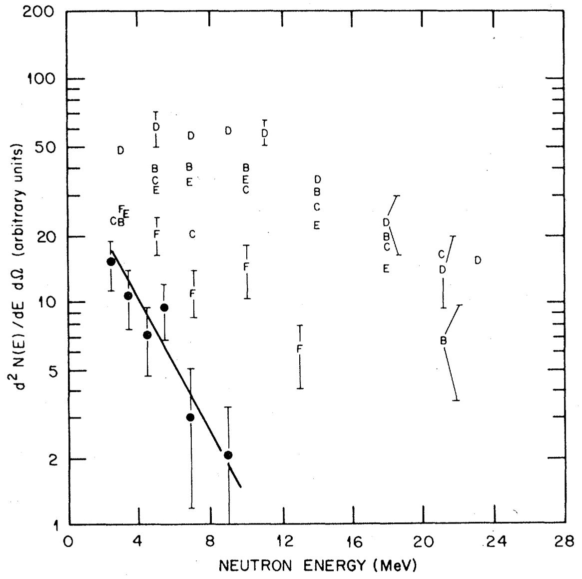

FIG. 13. Neutron spectra in coincidence with quasielastic projectilelike fragments from reactions between 160-MeV ^{13}C and ^{157}Gd. The letters designate the neutron counters (see Table I). Errors can be inferred from the fluctuations between adjacent points. The closed circles indicate combined results from background detectors *A* and *H*. The solid curve shows the result of a Monte Carlo evaporation calculation (see text).

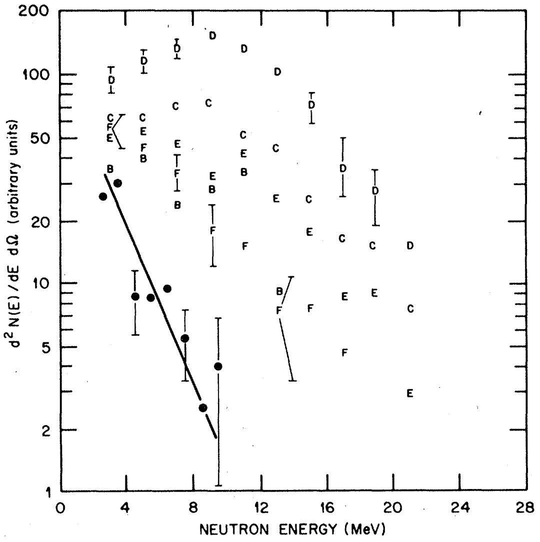

FIG. 14. Spectra of neutrons in coincidence with deeply inelastic products from reactions between 160-MeV ^{13}C and ^{157}Gd. Symbols are described in the caption of Fig. 13.

Because of the poor statistics, we are unable to provide detailed information on the neutron multiplicity in individual detectors as a function of the energy loss. In addition, results obtained in group (1) cannot be normalized because of insufficient coincidence statistics in our normalization run. (Most of the coincidence events were obtained while the singles events were being scaled down.)

Neutron spectra for group (1) are presented in

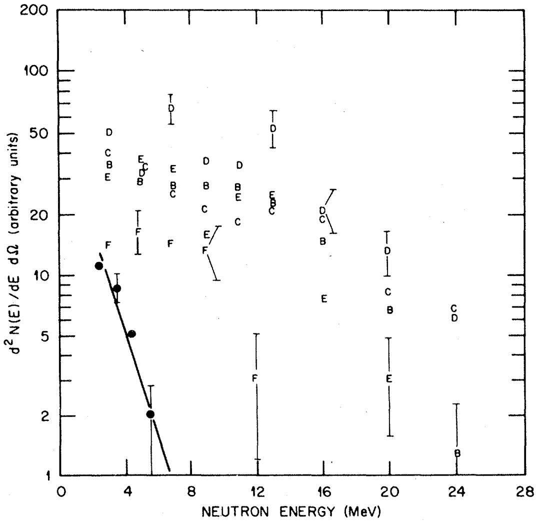

FIG. 15. Spectra of neutrons in coincidence with quasielastic products from reactions between 140-MeV ^{13}C and ^{157}Gd. For meaning of symbols see caption of Fig. 13.

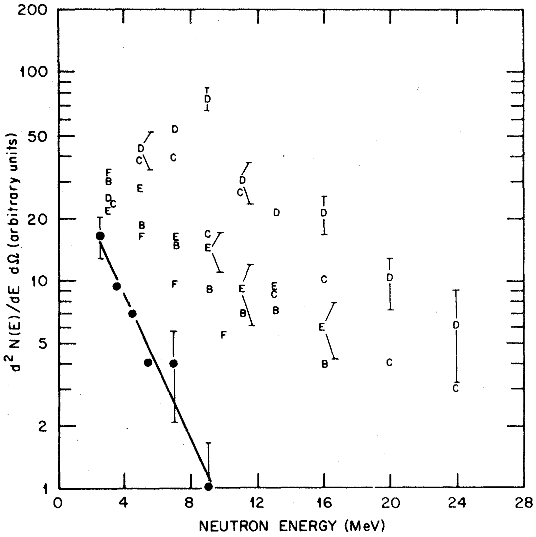

FIG. 16. Spectra of neutrons in coincidence with deeply inelastic products from reactions between 140-MeV ^{13}C and ^{157}Gd. For meaning of symbols see caption of Fig. 13.

Figs. 13—18. The data are presented separately for QE and DI events. The two categories were defined as follows. For 160-MeV ^{13}C the DI region covers a fragment kinetic energy range of 50—120 MeV and the QE region is 120—150 MeV. For 140-MeV ^{13}C the DI region ranges from 40 to 95 MeV and the QE region ranges from 95 to 130 MeV. For 150-MeV ^{12}C, DI events cover 50—110 MeV and QE events cover 110—140 MeV. We draw special attention to two features: (1) Detector *D*, situated between the PLF detector and the beam axis, has the largest number of

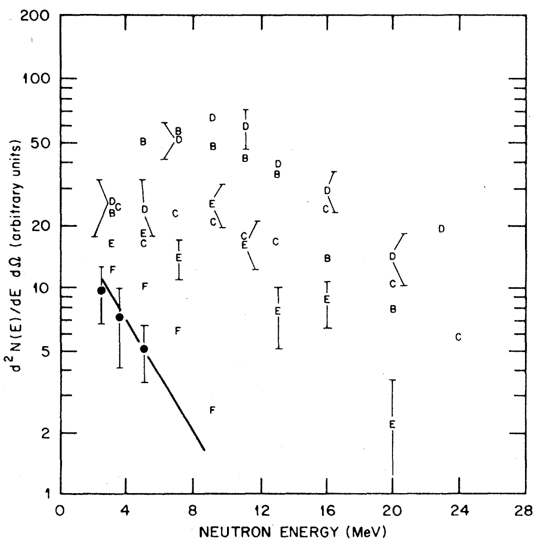

FIG. 17. Spectra of neutrons in coincidence with quasielastic products from reactions between 150-MeV ^{12}C and ^{158}Gd. For meaning of symbols see caption of Fig. 13.

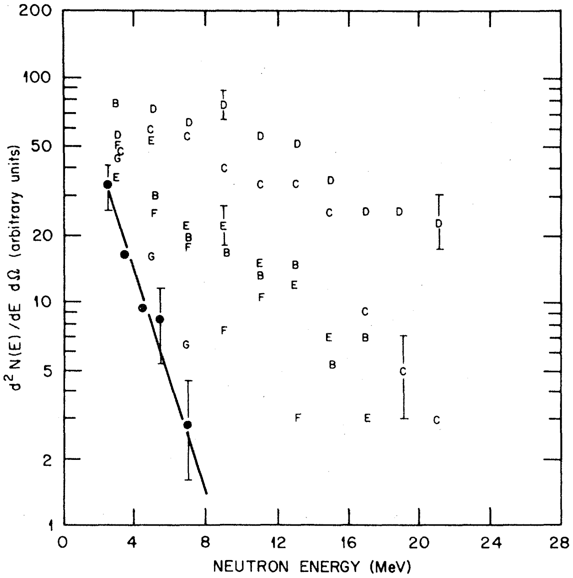

FIG. 18. Spectra of neutrons in coincidence with deeply inelastic products from reactions between 150-MeV ^{12}C and ^{158}Gd. For meaning of symbols see caption to Fig. 13.

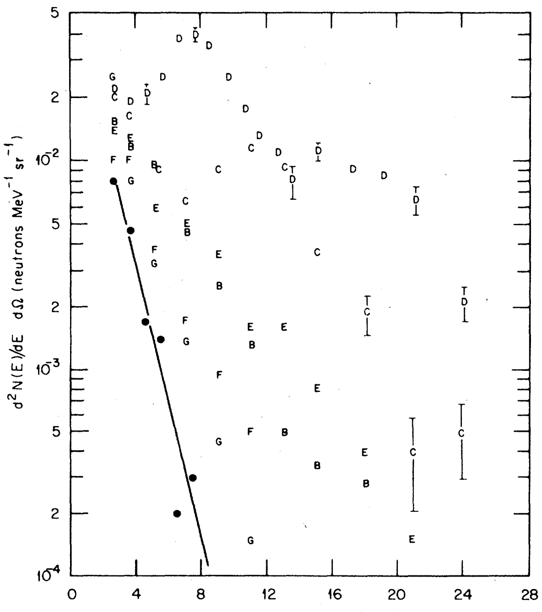

FIG. 19. Spectra of neutrons in coincidence with projectilelike fragments from reactions between 124-MeV ^{12}C and ^{158}Gd. For meaning of symbols see caption to Fig. 13.

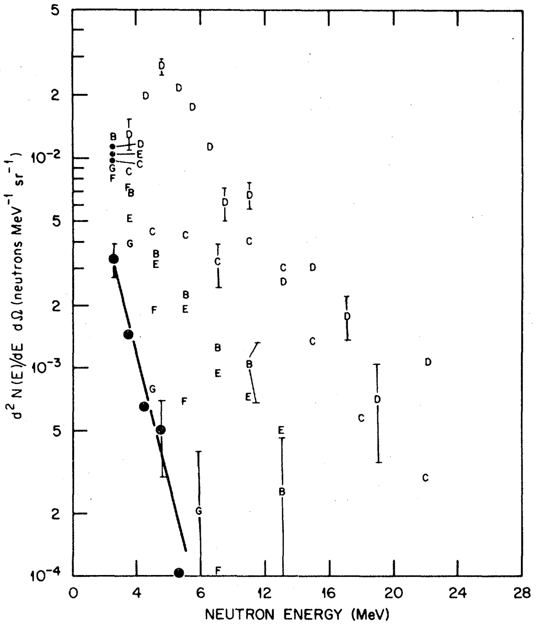

FIG. 20. Spectra of neutrons in coincidence with projectilelike fragments from reactions between 103-MeV ^{12}C and ^{158}Gd. For meaning of symbols see caption to Fig. 13.

events, and the spectrum has a broad peak around 10 MeV, falling off at higher energies. (2) The spectra in detectors *B*, *C*, *D*, and *E* are more closely bunched in the QE data than in the DI data; this is especially noticeable for the ^{13}C-induced reactions. We will discuss these points later.

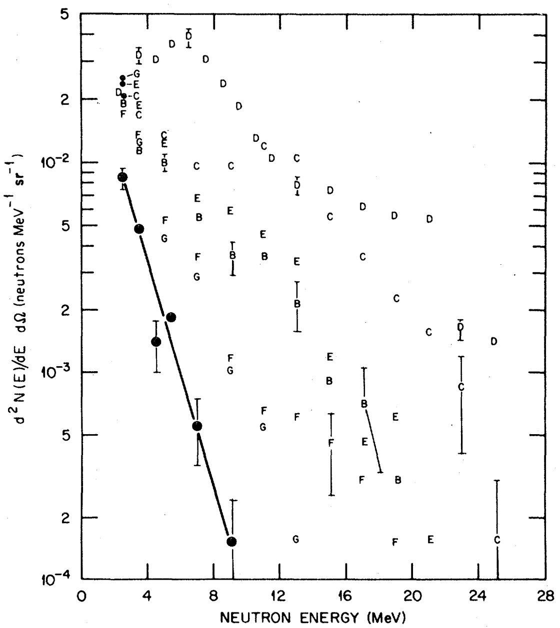

FIG. 21. Spectra of neutrons in coincidence with projectilelike fragments from reactions between 110-MeV ^{13}C and ^{157}Gd. For meaning of symbols see caption to Fig. 13.

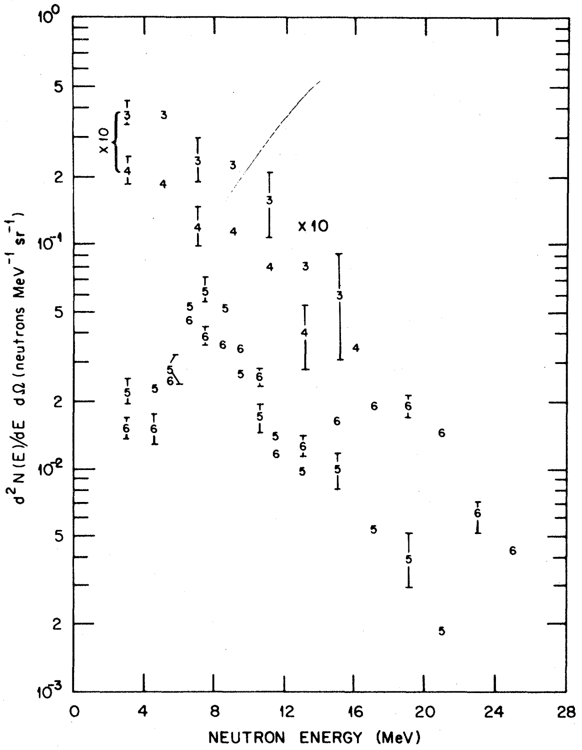

FIG. 22. Spectra of neutrons from detector *D* in coincidence with projectilelike fragments having specific values of *Z* from reactions between 124-MeV ^{12}C and ^{158}Gd. The numbers of the data points indicate the nuclear charge of the PLF with which the neutrons are in coincidence. Note the peaks in the neutron spectra associated with PLF's having $Z=5$ and $Z=6$.

Neutron spectra in coincidence with the PLF are presented for group (2) in Figs. 19—21. The most prominent feature of these results is a bump in the neutron spectra in detector *D* at an energy of 6—8 MeV. The average velocity of the neutrons that constitute this bump (3.4—3.9 cm/ns) is nearly the same as the average velocity of the PLF with which they are in coincidence (3.3—4.2 cm/ns). Figures 22—24 show neutron spectra in detector *D* for Li, Be, B, and C fragments. For ^{12}C the bump appears only in the boron and carbon channels, whereas for ^{13}C, the bump is discernible also in the Li and Be channels.

VI. DISCUSSION — NNE ASSOCIATED WITH INELASTIC REACTIONS

In most studies of neutron emission associated with inelastic heavy-ion reactions (Refs.

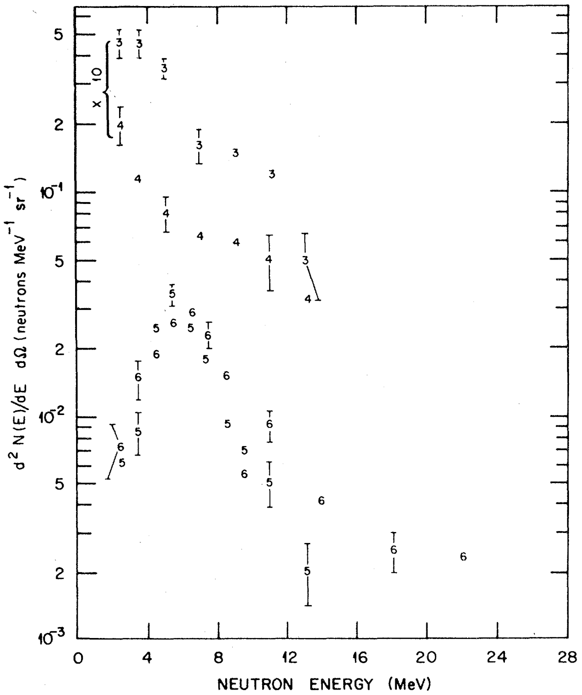

FIG. 23. Similar to Fig. 22, but from reactions between 104-MeV ^{12}C and ^{158}Gd.

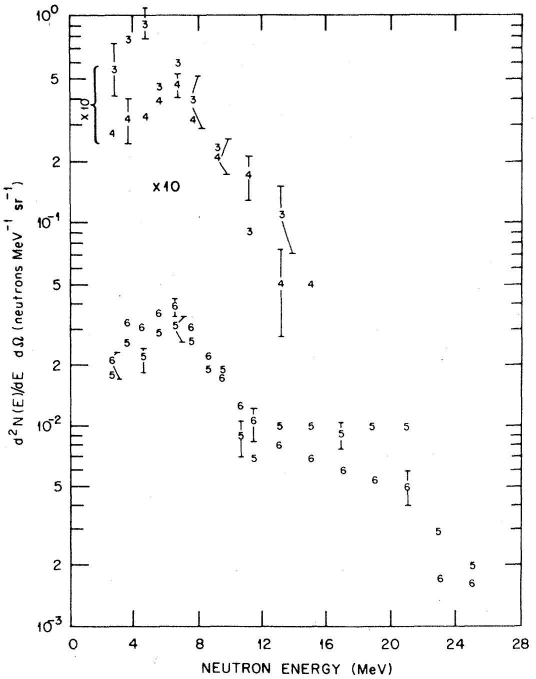

FIG. 24. Similar to Fig. 22, but from reactions between 110-MeV ^{13}C and ^{157}Gd.

20,23,24,28,29), the neutron spectra observed can be readily accounted for by assuming that the neutrons are evaporated from two fully accelerated sources, the TLF and the PLF. Only recently has evidence been presented in two cases that NNE may be associated with some DI reactions.[26,30] In the present case, neutrons evaporated from the slowly moving TLF are expected to be approximately isotropic in the laboratory, as the spectrum in that frame is transformed only slightly from that in the rest frame of the TLF. Neutrons emitted by fully accelerated PLF, on the other hand, are expected to have laboratory angular distributions strongly peaked at or near the direction of the PLF, especially in the case of QE events. Using known velocity distributions of the fragments and assuming two-body kinematics, we can calculate the expected neutron spectra with a Monte Carlo simulation procedure.

However, the representation of the spectrum of neutrons emitted by the PLF in our case poses problems not encountered in analysis of experiments involving heavier systems (Refs. 20,23,24,28,29). In these cases, excitation energy can be considered to be shared between the PLF and TLF in the ratio of their respective masses, on the assumption of equal temperatures for both fragments. It is then possible to describe the neutron emission spectra of the two fragments by the same Maxwell-Boltzmann distribution. In the present case, if we assume approximate equilibrium between the TLF and the PLF, the PLF is likely to have a low excitation energy ($\lesssim 10$ MeV) and a correspondingly low (often of the order of 1 MeV^{-1}) level density of the residual nucleus. For these reasons it is difficult to relate excitation energies to temperatures in the case of our projectilelike fragments. Consequently, it is possible that these fragments will not emit neutrons with a Maxwellian spectrum and that, in order to describe their neutron emission adequately, it will be necessary to take into account the distribution of states in the individual nuclei, as well as the widths of the levels and their variation with angular momentum.

Despite these difficulties, which may lead to problems when the details of the spectrum shapes are simulated, there exist definite correlations between the energies of neutrons emitted by the PLF and their angular distribution: High-energy neutrons emitted from the PLF should be detected in a wide angular range around its direction, whereas neutrons having a low energy in the PLF frame of reference will be detected only in a narrow cone around the PLF direction. For simplicity, we have performed a qualitative evaluation of the correlation between the c.m. neutron energy and the neutron angular distribution using Maxwellian-shaped neutron spectra for a number of different temperatures. Results of these calculations for 160-MeV $^{13}C+^{157}Gd$ are presented in Fig. 25. We note that for $T=0.5$ the shape of the high-energy tails for these spectra in detectors C and D are reasonably well reproduced (see Fig. 13). However, the calculations do not show a significant number of fast neutrons for detector E, which is contrary to experimental results. Calculations for $T \geq 1.5$ MeV do predict a relatively large yield of fast neutrons in detector E, but in this case the high-energy tail of the neutron spectrum for detector D extends to much higher energies than observed. Furthermore, none of the cases shown in Fig. 25 reproduce the relatively high neutron yield observed in detector B. Thus, the calculations, using a Maxwellian spectrum for the neutrons emitted by the PLF and containing the assumption that the emission takes place from fully accelerated PLF, cannot reproduce simultaneously the energy and angular variations of the spectra observed.

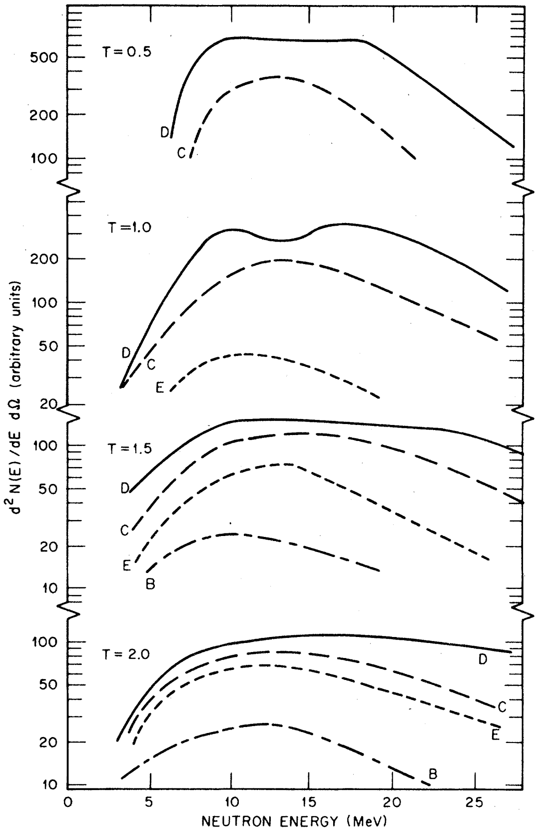

FIG. 25. Neutron spectra calculated for detectors B, C, D, and E by Monte Carlo techniques. The neutrons are assumed to be in coincidence with quasielastic fragments produced from reactions between 160-MeV ^{13}C and ^{157}Gd. T is the temperature parameter [Eq. (2), see text].

By contrasting the neutron spectra observed for QE with those for DI events from the same reaction, we obtain further indication that not all neutrons emitted by the PLF are emitted after it is fully accelerated. The DI fragment velocities are lower than those of QE products, and the available excitation energies for the deeply inelastic PLF are, therefore, probably higher than for QE events. Both these facts should cause the angular distribution of neutrons to be more nearly isotropic for DI than for QE events. Comparing Fig. 13 to 14, 15 to 16, and 17 to 18, we see that, generally, the opposite is true. The fragment angular distribution for QE events tends to peak at the grazing angle, which is near the PLF telescope angle for the cases of group (1) and somewhat inside it for the cases of group (2). (This situation can be contrasted with the forward-peaked distribution of DI products.) This could cause some of the observed bunching of neutron spectra for QE events, but not over the entire angular range observed for the neutrons.

We now consider a possible explanation of the peak in the neutron spectra located in the vicinity of 8 – 10 MeV. This peak is observed only in the data from detector D for group (2) experiments. In these group (2) experiments, detector D was located very nearly behind the PLF telescope (see Table I). A very strong correlation between the neutron and PLF emission directions clearly exists for this peak since it does not appear in adjacent neutron detectors, which are located at 23° (C) and at 48° (E) relative to the PLF direction. [The broad bump in detector D in group (1) experiments could be due to this same phenomenon. We suggest that it is significantly suppressed due to the 5° difference between the angle of detector D and the direction of the PLF.] In addition, the neutron velocity at the peak is approximately equal to that of the PLF. Evidently, in some events a neutron accompanies the PLF at a similar velocity. The multiplicity of these events is estimated to be very small. If we assume that all of the neutrons in this type of event are emitted into the solid angle of detector D (~ 25 msr), we obtain an overall multiplicity of six "neutron-accompanied" PLF's per 1000 events. We also recall (see Figs. 22 – 24) that these neutron-accompanied PLF's are isotopes with $Z=5$ or 6, but not with $Z=3$ or 4, for ^{12}C-induced reactions.

A possible explanation of the origin of the peaks

TABLE IV. Neutron-unbound states in PLF nuclei.

Parent nucleus	S_n[a] (MeV)	E^*[b] (MeV)	Γ[c] (keV)	$\theta_{\rm max}$[d]
^{7}Li	7.251	7.467	89 ± 7	9.6°
^{8}Li	2.033	2.261	36.5	9.8°
^{8}Be	18.900	18.91	48 ± 20	2.0°
^{9}Li	4.053	4.31	250 ± 30[e]	10.3°
^{9}Be[f]	1.6651	1.680	210 ± 25	2.5°
^{10}Be	6.8120	7.371	15.7	14.6°
^{10}B	8.435	8.889	84	13.3°
^{11}B	11.456	11.61	150 ± 50[g]	7.9°
^{12}B	3.369	3.3884	< 1.4[h]	2.8°
^{12}C	18.722	18.80	80 ± 30[i]	5.6°
^{13}B	4.880	5.023	?	7.5°
^{13}B	4.880	5.109	60 ± 8	9.6°
^{13}C	4.9464	9.498[j]	5	6.6°
^{14}C	8.1770	8.3183	3.4 ± 0.6	7.5°

[a] Neutron separation energy.

[b] Excitation energy of state.

[c] Width of state.

[d] Maximum opening angle of the emission cone (in the laboratory) of the neutron emitted by a PLF with 9 MeV/nucleon kinetic energy.

[e] $\Gamma_{\rm total}$.

[f] Note that this state would decay to unobserved $^{8}\mathrm{Be} \rightarrow \alpha + \alpha$.

[g] $\Gamma_n + \Gamma_\alpha$.

[h] $\Gamma_n = 3.1$ eV.

[i] $\Gamma_\gamma + \Gamma_n + \Gamma_p$.

[j] This state decays to the 4.439-MeV, 2^+ level in ^{12}C. The other states listed decay to the ground state of the daughter nucleus.

is that they are due to the decay of specific states in the PLF whose excitation energies are less than a few hundred keV above the neutron separation energy for the PLF nucleus involved. The decay of such states would result in neutron emission localized within a narrow cone about the direction of the PLF. Owing to the low kinetic energy released in the decay, the neutrons would have a narrow distribution of velocities centered about the PLF velocity. From considerations based on rotation frequencies and on the time required for Rutherford trajectories, we estimate the typical interaction time in our cases to be of the order of 5×10^{-21} s. If we initially require that the probability of decay of the excited state during this time be less than 10%, then the maximum permissible level width is about 15 keV.

In order to investigate further the possible explanation discussed above, we have examined known states[60] having finite neutron widths and involving low kinetic energy release for all nuclei with $Z = 3-6$ and $A = 6-15$. The levels with energies and widths that are closest to satisfying the above requirements are shown in Table IV. It can be seen that only levels in ^{12}B, ^{13}C, and ^{14}C actually satisfy the requirements. ^{12}B has a state at 3.3884 MeV (c.f. $S_n = 3.369$ MeV) with $\Gamma < 1.4$ keV; ^{13}C has a state at 9.498 MeV(c.f. $S_n = 4.9464$ MeV) with $\Gamma = 5$ keV that decays to ^{12}C at 4.439 MeV, and ^{14}C has a state at 8.3183 MeV (c.f. $S_n = 8.1770$ MeV) with $\Gamma_n = 3.4 \pm 0.6$ keV. The fact that suitable states exist only in boron and carbon may explain why the bumps observed are predominantly associated with PLF having $Z = 5$ and 6 for the ^{12}C-induced reactions.

If the above stringent requirements are relaxed slightly, it is seen that the states listed in Table IV for ^{7}Li, ^{8}Li, and ^{10}Be could also lead to peaks in detector D for events with $Z = 3$ or 4. These are, in fact, observed for ^{13}C-induced reactions (see Fig. 24). The difference between the ^{12}C and ^{13}C results (spectra associated with products of $Z = 3$ or 4 exhibit structure only in the latter case) may find an explanation in the differences between the primary mass distributions of the PLF, since that for ^{13}C is probably more neutron rich. We note that the absolute yield of neutrons is larger in the case of the ^{13}C-induced reactions, which is expected on the basis of the above considerations.

SUMMARY AND CONCLUSION

Nonequilibrium neutron emission associated with evaporation residues and with inelastic reactions has been studied in ^{12}C + ^{158}Gd and ^{13}C + ^{157}Gd reactions from 103 to 160 MeV. NNE was observed in all cases investigated. NNE associated with ER was successfully parametrized in terms of two moving sources. The velocity of the NNE source was found to increase with increasing bombarding energy, while the source temperature remained constant at about 4 MeV. No significant difference in NNE was observed between ^{12}C- and ^{13}C-induced reactions. The model of generalized critical angular momentum for partial fusion of Siwek-Wilczynska *et al.*[8] and the sum-rule generalization of this model by Wilczynski *et al.*[50] explained many aspects of our observations, such as the lack of a projectile structure effect, the observed NNE multiplicities, and the properties of the NNE source. Comparisons with the precompound decay model of Blann were made. The agreement between experiment and theory was poor in this case, but our results may provide valuable input to the further development of this model.

NNE associated with deeply inelastic and quasielastic reactions was also observed. It was not possible to obtain a parametrization of the results in terms of simple statistical emission from fully accelerated targetlike and projectilelike fragments. "Bumps" were observed in neutron spectra associated with certain projectilelike products, but only when the neutron detection angle was similar to the detection angle of the coincident PLF. An explanation of these bumps in terms of the excitation and decay of neutron-unbound levels with low kinetic energy release may be appropriate.

While further work is needed to broaden the data base with which model comparisons can be made, our results make a significant contribution to NNE systematics. It is our hope that the proponents of specific models of nonequilibrium emission will make use of the data presented here, as well as elsewhere, and examine the validity of their theories with reference to a broad range of systems.

ACKNOWLEDGMENT

This research was sponsored by the Division of High Energy and Nuclear Physics, U. S. Department of Energy, under Contract W-7405-eng-26 with the Union Carbide Corporation.

---

*Present address: Los Alamos National Laboratory, Los Alamos, New Mexico 87545.

†Present address: Oak Ridge National Laboratory, Oak Ridge, Tennessee 37830.

[1] M. Blann, Annu. Rev. Nucl. Sci. 25, 123 (1975).

[2] H. C. Britt and A. R. Quinton, Phys. Rev. 124, 877 (1961).

[3] J. Galin, B. Gatty, D. Guerreau, C. Rousset, U. C. Schlotthauer-Voos, and X. Tarrago, Phys. Rev. C 9, 1113 (1974); 9, 1126 (1974).

[4] M. L. Halbert, P. O. Tjom, I. Espe, G. B. Hagemann, B. Herskind, M. Neiman, and H. Oeschler, Nucl. Phys. A259, 496 (1976).

[5] T. Inamura, M. Ishihara, T. Fukuda, T. Shimoda, and H. Hiruta, Phys. Lett. 68B, 51 (1977).

[6] D. R. Zolnowski, H. Yamada, S. E. Cala, A. C. Kahler, and T. T. Sugihara, Phys. Rev. Lett. 41, 92 (1978).

[7] L. Westerberg, D. G. Sarantites, D. C. Hensley, R. A. Dayras, and J. H. Barker, Phys. Rev. C 18, 796 (1978).

[8] K. Siwek-Wilczynska, E. H. du Marchie van Voorthuysen, J. van Popta, R. H. Siemssen, and J. Wilczynski, Phys. Rev. Lett. 42, 1599 (1979); Nucl. Phys. A330, 150 (1979).

[9] H. Yamada, D. R. Zolnowski, S. E. Cala, A. C. Kahler, J. Pierce, and T. T. Sugihara, Phys. Rev. Lett. 43, 605 (1979).

[10] K. A. Geoffroy, D. G. Sarantites, M. L. Halbert, D.C. Hensley, R. A. Dayras, and J. H. Barker, Phys. Rev. Lett. 43, 1303 (1979).

[11] T. Inamura, T. Kojima, T. Nomura, T. Sugitate, and H. Utsunomiya, Phys. Lett. 84B, 71 (1979).

[12] P. Gonthier, H. Ho, M. N. Namboodiri, L. Adler, J.B. Natowitz, S. Simon, K. Hagel, R. Terry, and A. Khodai, Phys. Rev. Lett. 44, 1387 (1980).

[13] J. H. Barker, J. R. Beene, M. L. Halbert, D. C. Hensley, M. Jääskeläinen, D. G. Sarantites, and R. Woodward, Phys. Rev. Lett. 45, 424 (1980).

[14] H. Utsunomiya, T. Nomura, T. Inamura, T. Sugitate, and T. Motobayashi, Nucl. Phys. A334, 127 (1980).

[15] K. Geoffroy Young, D. G. Sarantites, J. R. Beene, M.L. Halbert, D. C. Hensley, R. A. Dayras, and J. H. Barker, Phys. Rev. C 23, 2479 (1981).

[16] H. Ho, R. Albrecht, W. Dunnweber, G. Graw, S. G. Steadman, J. P. Wurm, D. Disdier, V. Rauch, and F.

Scheibling, Z. Phys. A 283, 235 (1977).

[17] J. W. Harris, T. M. Cormier, D. F. Geesaman, L. L. Lee, Jr., R. L. McGrath, and J. P. Wurm, Phys. Rev. Lett. 38, 1460 (1977).

[18] C. -K. Gelbke, M. Bini, C. Olmer, D. L. Hendrie, J. L. Laville, J. Mahoney, M. C. Mermaz, D. K. Scott, and H. H. Wieman, Phys. Lett. 71B, 83 (1977).

[19] J. M. Miller, G. L. Catchen, D. Logan, M. Rajagopalan, J. M. Alexander, M. Kaplan, and M. S. Zisman, Phys. Rev. Lett. 40, 100 (1978).

[20] Y. Eyal, A. Gavron, I. Tserruya, Z. Fraenkel, Y. Eisen, S. Wald, R. Bass, G. R. Gould, G. Kreyling, R. Renfordt, K. Stelzer, R. Zitzmann, A. Gobbi, U. Lynen, H. Stelzer, I. Rode, and R. Bock, Phys. Rev. Lett. 41, 625 (1978); Phys. Rev. C 21, 1377 (1980).

[21] A. Gamp, J. C. Jacmart, N. Poffe, H. Doubre, J. C. Roynette, and J. Wilczynski, Phys. Lett. 74B, 215 (1978).

[22] R. K. Bhowmik, E. C. Pollacco, N. E. Sanderson, J. B. A. England, and G. C. Morrison, Phys. Rev. Lett. 43, 619 (1979).

[23] D. Hilscher, J. R. Birkelund, A. D. Hoover, W. U. Schröder, W. W. Wilcke, J. R. Huizenga, A. C. Mignery, K. L. Wolf, H. F. Breuer, and V. E. Viola, Jr., Phys. Rev. C 20, 576 (1979).

[24] B. Tamain, R. Chechik, H. Fuchs, F. Hanappe, M. Morjean, C. Ngo, J. Peter, M. Dakowski, B. Lucas, C. Mazur, M. Ribrag, and C. Signarbieux, Nucl. Phys. A330, 253 (1979).

[25] R. Billery, C. Cerruti, A. Chevarier, N. Chevarier, B. Cheynis, and A. Demeyer, Z. Phys. A 292, 293 (1979).

[26] G. A. Petitt, R. L. Ferguson, A. Gavron, F. E. Obenshain, F. Plasil, A. H. Snell, G. R. Young, K. A. Geoffroy, D. G. Sarantites, and C. F. Maguire, in *Proceedings of the International Symposium on Continuum Spectra of Heavy Ion Reactions, San Antonio, 1979* (Harwood Academic, New York, 1980), p. 319; A. Gavron, R. L. Ferguson, F. E. Obenshain, F. Plasil, G. R. Young, G. A. Petitt, K. Geoffroy Young, D. G. Sarantites, and C. F. Maguire, Phys. Rev. Lett. 46, 8 (1981).

[27] G. R. Young, R. L. Ferguson, A. Gavron, D. C. Hensley, F. E. Obenshain, F. Plasil, A. H. Snell, M. P. Webb, C. F. Maguire, and G. A. Petitt, Phys. Rev. Lett. 45, 1389 (1980).

[28] M. Dakowski, R. Chechik, H. Fuchs, F. Hanappe, B. Lucas, C. Mazur, M. Morjean, J. Peter, M. Ribrag, C. Signarbieux, and B. Tamain, Z. Phys. A 294, 289 (1980).

[29] C. R. Gould, R. Bass, J. V. Czarnecki, V. Hartmann, K. Stelzer, R. Zitzmann, and T. Eyal, Z. Phys. A 294, 323 (1980).

[30] H. Gemmeke, P. Netter, Ax. Richter, L. Lassen, S. Lewandowski, W. Lucking, and R. Schreck, Phys. Lett. 97B, 213 (1980).

[31] D. Logan, M. Rajagopalan, M. S. Zisman, J. M. Alexander, M. Kaplan, and L. Kowalski, Phys. Rev. C 22, 104 (1980).

[32] M. Bini, C. K. Gelbke, D. K. Scott, T. J. M. Symons, P. Doll, D. L. Hendrie, J. L. Laville, J. Mahoney, M. C. Mermaz, C. Olmer, K. Van Bibber, and H. H. Wieman, Phys. Rev. C 22, 1945 (1980).

[33] R. Babinet, B. Gauvin, J. Girard, J. M. Alexander, T. H. Chiang, J. Galin, B. Gatty, D. Guerreau, and X. Tarrago, Z. Phys. A 295, 153 (1980).

[34] M. B. Tsang, W. G. Lynch, R. J. Puigh, R. Vandenbosch, and A. G. Seamster, Phys. Rev. C 23, 1560 (1981).

[35] M. Blann, Nucl. Phys. A235, 211 (1974).

[36] M. Blann, Lawrence Livermore Laboratory Report UCRL-84526, 1980; Phys. Rev. C. (to be published).

[37] P.-A. Gottschalk and M. Westrom, Phys. Rev. Lett. 39, 1250 (1977).

[38] R. Weiner and M. Westrom, Nucl. Phys. A286, 282 (1977).

[39] P. -A. Gottschalk and M. Westrom, Nucl. Phys. A314, 232 (1979).

[40] S. I. A. Garpman, D. Sperber, and M. Zielinska-Pfabe, Phys. Lett. 90B, 53 (1980).

[41] W. W. Morrison, S. K. Samadarr, D. Sperber, and M. Zielinska-Pfabe, Phys. Lett. 93B, 379 (1980).

[42] D. H. E. Gross and J. Wilczynski, Phys. Lett. 67B, 1 (1977).

[43] J. P. Bondorf, J. N. De, A. O. T. Karvinen, G. Fai, and B. Jakobsson, Phys. Lett. 84B, 162 (1979).

[44] J. P. Bondorf, J. N. De, G. Fai, A. O. T. Karvinen, B. Jakobsson, and J. Randrup, Nucl. Phys. A333, 285 (1980).

[45] W. J. Swiatecki, Lawrence Berkeley Laboratory Report LBL-8950, 1979 (unpublished).

[46] M. C. Robel, Lawrence Berkeley Laboratory Report LBL-8181, 1979 (unpublished).

[47] Y. Boneh, A. Gavron, and S. Wald, Proceedings of the VII International Workshop on Gross Properties of Nuclei and Nuclear Excitations, Hirschegg, Austria, 1979 (unpublished).

[48] Y. Boneh and A. Gavron, in Volume of Contributed Papers, International Symposium on Continuum Spectra of Heavy Ion Reactions, San Antonio, 1979 (unpublished).

[49] T. Kishimoto and K. -I. Kubo, Progress in Research, April 1, 1978 to March 31, 1979, Cyclotron Institute, Texas A&M University (unpublished); Argonne National Laboratory Report ANL/PHY-79-4, 1979, p. 535 (unpublished).

[50] J. Wilczynski, K. Siwek-Wilczynska, J. van Driel, S. Gonggrijp, D.C.J.M. Hagemann, R. V. F. Jansens, J. Kukasiak, and R. H. Siemssen, Phys. Rev. Lett. 45, 606 (1980).

[51] T. Udagawa and T. Tamura, Phys. Rev. Lett. 45, 1311 (1980).

[52] D. G. Sarantites, L. Westerberg, M. L. Halbert, R. A. Dayras, D. C. Hensley, and J. H. Barker, Phys. Rev. C 18, 774 (1978).

[53] J. R. Beene, M. L. Halbert, D. C. Hensley, R. A. Day-

ras, K. Geoffroy Young, D. G. Sarantites, and J. H. Barker, Phys. Rev. C 23, 2463 (1981).

[54] M. Drosg, Nucl. Instrum. Methods 105, 582 (1972).

[55] M. Anghinofli, private communication.

[56] A. Gavron, Phys. Rev. C 17, 601 (1978).

[57] T. C. Awes, C. K. Gelbke, G. Poggi, B. B. Back, B. Glagola, H. Breuer, V. E. Viola, Jr., and T. J. M. Symons, Phys. Rev. Lett. 45, 513 (1980).

[58] M. Blann, private communication.

[59] G. R. Young, B. Cheynis, R. L. Ferguson, I. Y. Lee, R. Novotny, F. E. Obenshain, D. Pelte, F. Plasil, R. L. Robinson, C. F. Maguire, and G. A. Petitt (unpublished).

[60] F. Ajzenberg-Selove and T. Lauritsen, Nucl. Phys. A227, 1 (1974); F. Ajzenberg-Selove, *ibid.* A248, 1 (1975); A268, 1 (1976).

[61] A. Gavron, J. R. Beene, B. Cheynis, R. L. Ferguson, F. E. Obenshain, F. Plasil, G. R. Young, G. A. Petitt, M. Jääskeläinen, D. G. Sarantites, and C. F. Maguire (unpublished).